Pore-scale Modelling of Wettability Alteration during Primary Drainage

AGU PUBLICATIONS

Water Resources Research

RESEARCH ARTICLE
10.1002/2016WR018703

Pore-scale modeling of wettability alteration during primary drainage

W. Kallel[1], M. I. J. van Dijke[1], K. S. Sorbie[1], and R. Wood[2]

[1]School of Energy, Geoscience, Infrastructure and Society, Heriot-Watt University, Edinburgh, UK, [2]School of GeoSciences, University of Edinburgh, Edinburgh, UK

Key Points:
- A novel physically plausible wettability alteration model that occurs during primary drainage involving small polar compounds from the oil.
- Under certain conditions, the model enables the oil phase to achieve higher saturations (lower S_{wi}) at fixed maximum capillary pressures.
- The model presents a clear mechanism for the phenomenon of oil migration into the very small micropores in microporous carbonate rocks.

Supporting Information:
- Supporting Information S1
- Figure S1
- Figure S2
- Figure S3
- Figure S4
- Figure S5

Correspondence to:
M. I. J. van Dijke,
R.van_Dijke@hw.ac.uk

Citation:
Kallel, W., M. I. J. van Dijke, K. S. Sorbie, and R. Wood (2017), Pore-scale modeling of wettability alteration during primary drainage, *Water Resour. Res.*, *53*, 1891–1907, doi:10.1002/2016WR018703.

Received 1 FEB 2016
Accepted 2 FEB 2017
Accepted article online 7 FEB 2017
Published online 4 MAR 2017

Abstract While carbonate reservoirs are recognized to be weakly-to-moderately oil-wet at the core-scale, pore-scale wettability distributions remain poorly understood. In particular, the wetting state of micropores (pores <5 μm in radius) is crucial for assessing multiphase flow processes, as microporosity can determine overall pore-space connectivity. While oil-wet micropores are plausible, it is unclear how this may have occurred without invoking excessively high capillary pressures. Here we develop a novel mechanistic wettability alteration scenario that evolves during primary drainage, involving the release of small polar non-hydrocarbon compounds from the oil-phase into the water-phase. We implement a diffusion/adsorption model for these compounds that triggers a wettability alteration from initially water-wet to intermediate-wet conditions. This mechanism is incorporated in a quasi-static pore-network model to which we add a notional time-dependency of the quasi-static invasion percolation mechanism. The model qualitatively reproduces experimental observations where an early rapid wettability alteration involving these small polar species occurred during primary drainage. Interestingly, we could invoke clear differences in the primary drainage patterns by varying both the extent of wettability alteration and the balance between the processes of oil invasion and wetting change. Combined, these parameters dictate the initial water saturation for waterflooding. Indeed, under conditions where oil invasion is slow compared to a fast and relatively strong wetting change, the model results in significant non-zero water saturations. However, for relatively fast oil invasion or small wetting changes, the model allows higher oil saturations at fixed maximum capillary pressures, and invasion of micropores at moderate capillary pressures.

1. Introduction

Understanding the wettability characteristics of a porous medium is crucial in any effort to model carbon-dioxide trapping in aquifers or to optimize oil recovery in hydrocarbon reservoirs. Although wettability is known to be heterogeneous on a pore-to-pore scale [*Fassi-Fihri et al.*, 1995], current contact angle measurement techniques are unable to discriminate the pore-scale distribution of wettability in natural porous media. Imaging techniques such as Cryo-SEM [*Al-Yousef et al.*, 1995; *Fassi-Fihri et al.*, 1995] and Field-Emission SEM (FESEM) [*Dodd et al.*, 2014; *Knackstedt et al.*, 2011; *Marathe et al.*, 2012] can, however, be used for qualitative wettability analysis and attempts to identify wetting patterns. Examination of the wetting state of micropores is particularly important, as these may dominate the connected pore system in many carbonate reservoirs [*Cantrell and Hagerty*, 1999]. Moreover, although the contribution of the microporosity to both fluid flow and oil recovery has traditionally been thought to be unimportant, recent work has indicated that this may not be the case [*Harland et al.*, 2015; *Kallel et al.*, 2015].

We use the definition of micropores suggested by *Cantrell and Hagerty* [1999] as pores <5 μm in radius. There are common claims that micropores always maintain their strong affinity to water [*Fassi-Fihri et al.*, 1995]. Yet oil has been detected within micropores in carbonate rocks, making oil-wet conditions plausible [*Al-Yousef et al.*, 1995; *Clerke*, 2009; *Clerke et al.*, 2014; *Dodd et al.*, 2014; *Fung et al.*, 2011; *Knackstedt et al.*, 2011]. An oil-wet state may have developed either over geological time in large oil columns where high enough capillary pressures are reached, or as remnant distributions in initially larger pores, or if the micropores undergo progressive wettability changes.

Wettability alteration is often said to be associated with asphaltenes, which have been cited as being major wetting alteration agents. Asphaltenes are high molecular weight polar aggregates occurring in many crude

oils, coated by lower molecular weight molecules called resins. The large average size of $\sim$0.6 μm of the asphaltenes is thought to prevent them from accessing micropores of their own size [*Al-Yousef et al*., 1995]. In addition, asphaltenes have the characteristic of being insoluble in water (hydrophobic). This prevents them from penetrating protective water films and directly contacting the pore walls. However, if the protective stable water film breaks down to a molecularly thin film, for instance by reaching high enough capillary pressures, asphaltenes may then irreversibly adsorb onto the surface, hence rendering it oil-wet [*Kovscek et al*., 1993]. The thicker water films may initially be destabilized by the adsorption of smaller molecular weight polar components present in the crude oil. According to *Buckley and Liu* [1998], several mechanisms may be responsible for the adsorption of components from the oleic phase: polar interactions, surface precipitation, acid/base interactions and ion binding.

A complementary theory suggests that the thin water films may initially be destabilized by the adsorption of polar components with smaller molecular weight that are present in the crude oil [*van Duin and Larter*, 2001; *Bennett et al*., 2004]. Indeed, crude oils are usually rich in smaller polar nonhydrocarbon compounds, for instance the aromatic oxygen compounds such as alkylphenols (e.g., phenol C_0-C_3) [*Lucach et al*., 2002; *Taylor et al*., 1997]. Alkylphenols are characterized by their high solubility in water (hydrophilic, unlike asphaltenes) and high surface activity. Indeed, *Huang et al*. [1996] induced wetting changes in a laminated rock using a "synthetic crude oil" containing a number of candidate smaller polar molecules such as cresols, phenols, carbazoles, methylquiniline, etc. *Van Duin and Larter* [2001] used molecular dynamics simulations to suggest a wettability alteration process involving these small water-soluble polar nonhydrocarbon compounds. First, they penetrate the water films coating water-wet mineral surfaces. They then rapidly adsorb onto the surface and render it more hydrophobic. As a result, the water film is disrupted and the disjoining pressure is lowered thus making the film prone to collapse at the existing local oil/water capillary pressure. This water film collapse then allows direct contact with the surface by heavier compounds, such as asphaltenes. As a result, the surface is rendered oil wet.

Bennett et al. [2004] confirmed this wettability alteration process in a core-flood experiment on a sandstone, where they observed an early rapid wettability alteration that occurred during primary drainage involving alkylphenols. Indeed, these small polar species were absent from the eluted oils at the end of the experiment. The nonappearance of polar compounds is mainly due to their high interaction with the surface, which decreased across the length of the core. This resulted in a significant wettability alteration, preferentially near the inlet, confirmed by an ESEM (Environmental SEM) examination of the core after wetting alteration. Additionally, the authors pointed out the relative speed of the process, which may happen in a reservoir over a time scale from days to months. Thus, the time scale of wetting alteration in such a mechanism would depend on the slowest step in the process from diffusion of the polar organics into the water films, the adsorption of these smaller polar molecules to the rock surface, the lowering of the disjoining pressure of the water film and its subsequent collapse and finally the adhesion of larger polar compounds such as asphaltenes onto the rock surface.

In a previous paper, we examined a physically based wettability alteration model to describe wettability distributions and their consequences in pore network models [*Kallel et al*., 2015]. This earlier work described in a simple manner the rule-based wetting change mechanism that strictly occurs *following* ageing in crude oil due to the surface adsorption of such species as asphaltenes. This corresponds to the traditional approach that mimics the three-stage process experienced by an initially water-wet reservoir: primary drainage, ageing and waterflood.

In this work, we present a more mechanistic physically plausible model for the initial stages of wetting change from water-wet to more intermediate-wet conditions, which may occur *during* primary drianage (PD). We implement the model in a quasi-static pore network model to explain and numerically simulate the wettability alteration mechanism suggested by *Bennett et al*. [2004] involving small polar compounds from the oil. We have added a "scaled" time-dependency to the common oil invasion-percolation algorithm to be able to incorporate a time-dependent transport model for polar compounds. The time scaling referred to incorporates the balance between the oil invasion/migration time scale and the time scale of diffusion of small polar species and their adsorption which triggers a wetting change. The physical and chemical processes in this model will affect the final phase distributions and initial water saturations in the oil column after oil migration. Particularly, the model provides a clear and precise mechanism of how oil can migrate into micropores, without necessarily reaching the excessively high capillary pressures that would be required for oil invasion into

strongly water-wet micropores. However, the current model stops short of the full "ageing" change associated with asphaltenes and the resulting oil-wet conditions, but this further process and its effect on subsequent imbibition will be considered in a forthcoming paper. In section 2, details are given of how small polar nonhydrocarbon molecules diffuse from the oil into and through the water phase within the pore network, thus leading to wettability alteration which can progress as the primary drainage process occurs. In section 3, we present the resulting fluid distributions at the pore level (pore occupancies) and the consequences of these changes on the phase saturation profiles within the oil column during primary drainage. These calculations are based on two networks with distinct pore structures; the first is based on the digital pore network of a relatively simple Berea sandstone [*Jiang et al.*, 2007] and the second is a multiscale network of macropore and micropore generated from a carbonate rock sample [*Jiang et al.*, 2013].

2. Model Description

The model developed in this work is an extension of the quasi-static two-phase flow network modeling tool that has been described previously by *Ryazanov et al.* [2014] and *Kallel et al.* [2015]. The model starts with initially water-filled and perfectly water-wet pores, with the initial oil/water contact angle, $\theta=0^{\circ}$. Commonly in quasi-static pore network modeling simulators, oil invasion occurs pore by pore at discrete invasion percolation (IP) events. These are assumed to happen instantaneously, hence time is not explicitly taken into consideration. In this work, we separate these invasion events in time, based on an assumed flow rate Q, corresponding to a charge time for an oil reservoir by oil migration, as illustrated in supporting information Figure S1.

In fact, we assume that the invading volumes of oil, V_{oil} $[\mathrm{m}^3]$ linearly increase over time: $V_{oil}(t)=Q*t$, where $t[\mathrm{s}]$ is the migration time; Q $[\mathrm{m}^3\mathrm{s}^{-1}]$ is the flow of hydrocarbons invading a reservoir rock. Q is chosen low enough to remain in the capillary-dominated regime, i.e., the capillary number satisfies the following condition [*Blunt and Scher*, 1995]:

$$N_c=\frac{q\mu}{\sigma_{ow}}\leq 10^{-4} \tag{1}$$

where μ is the viscosity and σ_{ow} the oil-water interfacial tension, and $q=Q/A_{inlet}$, with A_{inlet} the total cross-sectional area at the system inlet. We effectively replace a discrete process which occurs in steps by a continuous process described by a straight line.

At time t_i during instantaneous oil invasion of pore i, we consider the polar compounds to be transported through the oil phase. The details of this process are provided in section 2.1. Additionally, during the period of time $t_{i+1}-t_i$ separating two successive pore invasion events, a diffusion/adsorption model for polar compounds is applied using discrete time steps, Δ_t^{TR}. In fact, we assume that the polar compounds diffuse to—and adsorb in—the oil-filled pores, as well as in the water-filled pores due to their high solubility in water [*Bennett et al.*, 2004], as detailed in section 2.2. The initial conditions for the diffusion/adsorption process are related to the oil/water configuration and their relative concentrations at time t_i.

2.1. Transport Through Oil Invasion

Throughout this section, we will consider a single pore i and define $C_{i_o}(\mathrm{t})$ $\left[{}^{\mathrm{mg}}/_{\mathrm{L}}\right]$ and $C_{i_w}(\mathrm{t})$ $\left[{}^{\mathrm{mg}}/_{\mathrm{L}}\right]$ as the mobile concentrations of polar compounds in the oil phase and water phase, respectively, and $\Gamma_i(\mathrm{t})$ $\left[{}^{\mathrm{mg}}/_{\mathrm{m}^2}\right]$ as the corresponding adsorption level of polar compounds per unit area in pore i at time t. Note that we assume perfect mixing within each phase.

If pore i is water-wet and has corners, water remains in the pore corners, as well as in a thin film lining the pore wall following oil invasion [*Kovscek et al.*, 1993]. When polar compounds are transported into the oil phase of pore i, either through oil invasion or through diffusion, we assume that they instantaneously partition between the oil and water phases within the same pore, since they are highly soluble in water, and that they instantly adsorb onto the surface from the water phase. These are reasonable assumptions given the time scales of diffusion and adsorption with the relatively slower migration of oil. An illustration of the partitioning and adsorption within an angular oil-filled pore is shown in supporting information Figure S2. We also assume that the concentration of polar compounds in the water phase, $C_{i_w}(\mathrm{t})$, is linearly related to the oil phase concentration, $C_{i_o}(t)$, as follows:

$$C_{i_w}(t) = PC_{i_o}(t), \quad \forall t > 0 \tag{2}$$

where P is the partitioning coefficient, input to the model ($0 < P < 1$).

During oil invasion of pore i at time t_i, we consider the polar compounds to be carried by the oil phase. Hence, we assume that $C_{i_o}(t_i)$ is equal to the concentration at the oil invasion front, computed as an average of the oil phase concentrations in the adjacent oil-filled pores:

$$C_{i_o}(t_i) = \frac{\sum_{k=1}^{z_o} C_{k_o}(t_i) V_{k_o}}{\sum_{k=1}^{z_o} V_{k_o}} \tag{3}$$

We define V_{k_o} and V_{k_w} as the volumes of the oil phase and water phase of pore k, respectively, satisfying $V_{k_o} + V_{k_w} = V_k$. Besides, z_o is the number of oil-filled pores adjacent to pore i, $z_o \leq z$, where z is the total number of pores connected to pore i; z is equal to 2 for a bond, corresponding to its two connecting nodes ($z=1$ for a boundary bond) and $z \geq 1$ for a node, corresponding to its coordination number (number of neighboring bonds).

Immediately after oil invasion of pore i at time t_i, the total mass within the pore, $m_i(t_i)$, is equal to $C_{i_o}(t_i) * V_{i_o} + C_{i_w}(t_i) * V_{i_w} + \Gamma_i(t_i) * SA_i$, where SA_i $[m^2]$ is the total surface area of the pore. Since both the partitioning and adsorption are instantaneous, this mass is supposed to instantaneously distribute between the phases within the same pore and to adsorb onto the surface in accordance with a Langmuir isotherm. This happens straight afterward (at t_i^+), as follows:

$$\Gamma_i(t_i^+) = \Gamma_{\max} \frac{KC_{i_w}(t_i^+)}{1 + KC_{i_w}(t_i^+)}$$

$$m_i(t_i^+) = C_{i_o}(t_i^+) * V_{i_o} + C_{i_w}(t_i^+) * V_{i_w} + \Gamma_i(t_i^+) * SA_i = m_i(t_i) \tag{4}$$

where $\Gamma_{\max}[mg/m^2]$ and $K[L/mg]$ are the Langmuir maximum adsorption level per unit area and adsorption constant, respectively.

By combining equations (2) and (4), we obtain a single quadratic equation that we solve for $C_{i_o}(t_i^+)$, knowing $C_{i_o}(t_i)$, $C_{i_w}(t_i)$, and $\Gamma(t_i)$:

$$KP.C_{i_o}(t_i^+)^2 + \left(1 + \frac{KP}{V_{i_o} + PV_{i_w}} (\Gamma_{\max}.SA_i - m_i(t_i))\right).C_{i_o}(t_i^+) - \frac{m_i(t_i)}{V_{i_o} + PV_{i_w}} = 0 \tag{5}$$

Afterward, $C_{i_w}(t_i^+)$ and $\Gamma_i(t_i^+)$ are directly derived from equations (2) and (4), respectively.

2.2. Transport Through Diffusion

As previously stated, polar compounds diffuse into both oil-filled and water-filled pores during the period of time separating two successive pore invasions at discrete time steps Δ_t^{TR} .

2.2.1. Mass Balance Equations

2.2.1.1. Oil-Filled Pores

The material balance of the polar compounds within pore i is described by the diffusion-adsorption equation in the following from, discretized along the network structure:

$$\frac{\Delta C_{i_o}}{\Delta_t^{TR}} = \frac{C_{i_o}(t + \Delta_t^{TR}) - C_{i_o}(t)}{\Delta_t^{TR}} = \frac{1}{V_{i_o} \Delta_t^{TR}} (\Delta m_{d_i} - \Delta m_{ex_i})$$

$$\frac{\Delta C_{i_w}}{\Delta_t^{TR}} = \frac{C_{i_w}(t + \Delta_t^{TR}) - C_{i_w}(t)}{\Delta_t^{TR}} = \frac{1}{V_{i_w} \Delta_t^{TR}} (\Delta m_{ex_i} - \Delta m_{a_i}) \tag{6}$$

where Δm_{d_i}, Δm_{ex_i} and $\Delta m_{a_i}[mg]$ are the masses of polar compounds that diffused into the bulk phase (here oil), that exchanged between the oil and the water phases and that adsorbed onto the surface, respectively, in pore i during time increment $\Delta_t^{TR}[s]$; Additionally, we assume that the diffusion occurs only through the bulk phase, neglecting any mass exchanged with the neighboring pores through the corner water phase. Since Δm_{ex_i} is the same mass exchanged between oil and water, the two equations in (6) lead to a single equation:

$$V_{i_o}\left(C_{i_o}\left(t+\Delta_t^{TR}\right)-C_{i_o}(t)\right)+V_{i_w}\left(C_{i_w}\left(t+\Delta_t^{TR}\right)-C_{i_w}(t)\right)=\Delta m_{d_i}-\Delta m_{a_i} \tag{7}$$

2.2.1.2. Water-Filled Pores

Additionally, due to their supposedly high water solubility, polar compounds are assumed to diffuse into the water-filled pores where they also adsorb onto the surface. Since the pore only contains a water phase, the material balance for the polar compounds is simply provided by the following equation:

$$\frac{\Delta C_{i_w}}{\Delta_t^{TR}}=\frac{C_{i_w}\left(t+\Delta_t^{TR}\right)-C_{i_w}(t)}{\Delta_t^{TR}}=\frac{1}{V_i\Delta_t^{TR}}\left(\Delta m_{d_i}-\Delta m_{a_i}\right) \tag{8}$$

2.2.2. Diffusion Model

We apply a discretized form of Fick's diffusion equations for the diffusion of polar compounds within pore i (equation (9)), with the diffusion front only advancing to the directly adjacent pores ahead at each time step Δ_t^{TR}.

$$\Delta m_{d_i}=\Delta_t^{TR}\sum_{k=1}^{z}J_{ki}.\min\left(A_i,A_k\right)$$

$$J_{ji}=-D\frac{C_i(t)-C_j(t)}{L_{ji}} \tag{9}$$

where z is the number of pores connected to pore i (as defined above); J_{ji} $\left[{}^{\mathrm{mg}}/_{\mathrm{m^2s}}\right]$ is the diffusion flux from pore j to pore i, which occurs across the minimum bulk-phase cross-sectional area, A $[\mathrm{m}^2]$, between the two adjacent pores; L_{ji} $[\mathrm{m}]$ is the distance between the centre of pore j and center of pore i; D $\left[\mathrm{cm}^2/\mathrm{s}\right]$ is the diffusion coefficient. Note that at fixed physical diffusion coefficient D, we should carefully choose a low Δ_t^{TR} in order to avoid instabilities that arise from the discretized diffusion model. Indeed, unless every pore satisfies the condition below, mass conservation fails:

$$\Delta m_{d_i}+m_{i_{bulk}}(t)\geq 0 \tag{10}$$

where *bulk* corresponds to the pore's bulk phase, through which the diffusion occurs; and $m_{i_{bulk}}(t)$ is the mass in the bulk phase at the beginning of the time step (initial), defined as $m_{i_{bulk}}(t)=C_{i_{bulk}}(t)V_{i_{bulk}}$.

As for the boundary conditions, the concentration at the inlet is taken as constant over time, equal to C_0. At the outlet, a "no flow" boundary condition is assumed.

We model the diffusion between two pores sharing the same bulk phase using the bulk-phase concentrations, i.e., the diffusion from oil to oil-filled and water to water-filled pores is computed in equation (9) using $C_{i_o}(t)-C_{j_o}(t)$ and $C_{i_w}(t)-C_{j_w}(t)$ respectively. For the case of cross-phase diffusion, i.e., from water to oil-filled pores and vice versa, we use the difference in water concentrations: $C_{i_w}(t)-C_{j_w}(t)$. Indeed, we assume that the polar compounds partition first from the oil to the water phase at the interface between two adjacent pores, then they diffuse within the water phase. In this particular case, L_{ji} is taken as only half the length of the water-filled pore. An illustration of the diffusion mechanism is provided in supporting information Figure S3.

2.2.3. Adsorption Model

The adsorption of polar compounds is assumed to occur from the water phase instantaneously. However, since the polar compounds concentration changes through diffusion at discrete time steps Δ_t^{TR}, adsorption is only computed at each Δ_t^{TR}. It is described by a Langmuir isotherm which has the following form:

$$\Delta m_{a_i}=SA_i\left(\Gamma_i\left(t+\Delta_t^{TR}\right)-\Gamma_i(t)\right)$$

$$\Gamma_i\left(t+\Delta_t^{TR}\right)=\Gamma_{\max}\frac{KC_{i_w}\left(t+\Delta_t^{TR}\right)}{1+KC_{i_w}\left(t+\Delta_t^{TR}\right)} \tag{11}$$

2.2.4. Equations Summary

2.2.4.1. Oil-Filled Pores

To summarize, in an oil-filled pore i at $t+\Delta_t$, we have $\Delta m_{d_i}=\Delta m_{d_i}(C_i(t))$ and $\Delta m_{a_i}=\Delta m_{a_i}\left(\Gamma_i(t),\ \Gamma_i\left(t+\Delta_t^{TR}\right),\ C_{i_w}\left(t+\Delta_t^{TR}\right)\right)$. Knowing $\Gamma_i(t)$, $C_{i_o}(t)$ and $C_{i_w}(t)$ from the previous time step, we combine equations (7), (9), and (11) to obtain a single quadratic equation that we solve for $C_{i_o}\left(t+\Delta_t^{TR}\right)$:

$$KP.C_{i_o}\left(t+\Delta_t^{TR}\right)^2+\left(1-KPB+\frac{\Gamma_{\max}KP.SA_i}{V_{i_o}+PV_{i_w}}\right).C_{i_o}\left(t+\Delta_t^{TR}\right)-B=0 \tag{12}$$

where $B=C_{i_o}(t)+\frac{\Delta m_{d_i}+\Gamma_i(t).SA_i}{V_{i_o}+PV_{i_w}}$.

Afterward, $C_{i_w}\left(t+\Delta_t^{TR}\right)$ and $\Gamma_i\left(t+\Delta_t^{TR}\right)$ are directly derived from equations (2) and (11), respectively. Since the concentration of polar compounds in the inlet is constant, equal to C_0, C_{i_o} and C_{i_w} increase from 0 to C_0 and PC_0, respectively, following the transport model.

2.2.4.2. Water-Filled Pores

Similarly, for a water-filled pore i, we combine equations (8), (9), and (11), and solve for the unknown $C_{i_w}\left(t+\Delta_t^{TR}\right)$:

$$K.C_{i_w}\left(t+\Delta_t^{TR}\right)^2+\left(1-KB+\frac{\Gamma_{\max}K.SA_i}{V_i}\right).C_{i_w}\left(t+\Delta_t^{TR}\right)-B=0 \tag{13}$$

where $B=C_{i_w}(t)+\frac{\Delta m_{d_i}+\Gamma_i(t).SA_i}{V_i}$.

$\Gamma_i\left(t+\Delta_t^{TR}\right)$ is directly derived from equation (11). Besides, C_{i_w} increases from 0 to PC_0 following the transport model.

2.3.5. Wettability Alteration

Due to the polar species adsorption, the pore surface undergoes a wettability alteration [*Bennett et al.*, 2004]. In the absence of any comprehensive model that links the adsorption of polar compounds to the wettability change, we simply assume that the cosine of the contact angle changes as a linear function of the adsorption level of polar compounds:

$$\cos\theta_i=1-(1-\beta)\frac{\Gamma_i}{\Gamma_{\max}} \tag{14}$$

While $\Gamma_i=0$, the initial contact angle remains unchanged, i.e., $\cos\theta_i=1$. Note that β is an input parameter ranging between 0 and 1, and corresponds to the limiting contact angle value where $\Gamma_i=\Gamma_{\max}$. However, in accordance with the Langmuir adsorption isotherm in equation (11), the actual maximum value $\Gamma_{\max\_actual}$ that Γ_i can reach as the transport model is carried out is:

$$\Gamma_{\max\_actual}=\Gamma_{\max}\frac{KPC_0}{1+KPC_0} \tag{15}$$

Hence, by combining equations (14) and (15), $\cos\theta_i$ decreases during the simulation from 1 to a minimum value, related to a maximum contact angle $\theta_{\max}$:

$$\cos\theta_{\max}=\frac{1+\beta KPC_0}{1+KPC_0} \tag{16}$$

Consequently, β can be defined as $\beta=\cos\theta_{\max}(K\rightarrow+\infty)$ at finite C_0 (or as $\cos\theta_{\max}(C_0\rightarrow+\infty)$ at finite K). We identify two distinct effects of the wetting change in the oil-filled and water-filled pores.

2.3.5.1. Oil-Filled Pores

Due to the uniform contact angle change in any angular pore i, the amount of water in the corners decreases if the water is connected to the outlet. Water may be completely expelled from the pore if it satisfies condition (17), as illustrated in supporting information Figure S4.

$$\theta_i>\frac{\pi}{2}-\gamma_i \tag{17}$$

where γ_i is the half-angle of the angular cross sections.

A direct consequence of this mechanism is that water may get surrounded by oil in the vicinity of the water films collapse, which generates trapping of water in the network. In fact, the water phase connectivity may drop significantly at this stage due to large contact angle changes.

2.3.5.2. Water-Filled Pores

As the adsorption levels increase during the transport process in a water-filled pore i adjacent to the oil front, the contact angle increases. Consequently, the pore entry pressure, P_E, decreases, which makes the pore more prone to oil invasion. Oil may then spontaneously invade pore i when its wettability has changed enough for its entry pressure, P_E, to decrease below the current capillary pressure value P_c.

The simulation is stopped when no more invasions are possible at a predefined maximum capillary pressure, $P_c^{\max}$ and the adsorption steady state is reached. The adsorption steady state is defined as the

condition where all the remaining accessible and nontrapped water-filled pores have adsorbed their maximum capacity of polar compounds, i.e., their contact angles have reached a final value equal to θ_{max} (equation (16)). The ultimate water saturation obtained at the predefined P_c^{max} will simply be referred to as S_{wi} (corresponding to an oil saturation $S_{oi}=1-S_{wi}$), which is reached at a final time denoted as t_f. We refer to the newly developed model of Primary Drainage during which a Wettability Evolution occurs as PD/WE. An example of the first steps of the simulation is carried out on a regular 2-D network and shown in supporting information Figure S5. It illustrates the various processes involved in the PD/WE model.

3. Results and Discussion

The simulations are performed on the two networks presented and used by *Kallel et al.* [2015]: a fairly homogeneous Berea sandstone network [*Jiang et al.*, 2007], and a heterogeneous network derived from a microporous carbonate dataset [*Jiang et al.*, 2013]. The Berea and carbonate networks are characterized by total numbers of pore elements equal to 22,251 and 26,349, average coordination numbers of 3.7 and 3.5, overall porosities of 19% and 21%, and absolute permeabilities of 1576 and 59 mD, respectively. As described by *Kallel et al.* [2015], each network consists of pores with different cross-sectional geometries including regular n-cornered polygons and stars. Note that the five-cornered star shapes are predominant in both networks, with their corresponding half-angle γ ranging between 5 and 54°. The latter value corresponds to the pentagon shape.

In this work, we link the pore-scale simulations to the reservoir scale. In fact, we associate each P_c reached locally in the network with a corresponding height, h, in the oil column:

$$h=\frac{P_c}{\Delta\rho.g} \tag{18}$$

where $\Delta\rho=\rho_w-\rho_o$ denotes the difference between the fluids volumetric mass densities (here chosen as 0.2 kg/L); g denotes gravity (9.81 m/s^2).

Actually, two main effects will be demonstrated in our simulations, both of which dictate the initial water saturation for waterflooding, S_{wi}:

1. The effect of the contact angle, θ_{max} on S_{wi}: while K, P and C_0 are kept constant, β is varied to induce changes in the contact angles (equation (16)). We either assign a unique β throughout the network, corresponding to a single θ_{max} for all the pores, or uniformly distribute β among the pores, generating a range of contact angles θ_{max}.
2. The effect of the balance between oil invasion and wettability alteration on S_{wi}: while we keep the oil flow rate, Q, constant, we vary the maximum adsorptive capacity, Γ_{max}. Hence, the polar compounds adsorption level required to reach the fixed maximum contact angle θ_{max} is changed (equation (14)). This induces changes in the balance between the processes of oil invasion and wettability alteration.

Note that for the latter sensitivity study at fixed θ_{max}, two limiting cases arise:

1. In the case of an extremely fast wettability alteration relative to flow rate, a full wetting change within every pore precedes its invasion by oil. Hence, we can simply model it as a conventional PD with an initial contact angle equal to θ_{max}. We call this special case the Fast Wetting Boundary (FWB).
2. If the oil flow rate is much faster than the wetting change, all invasions are supposed to happen instantaneously. The oil invasion process is carried out until the imposed maximum capillary pressure, P_c^{max}, is reached. Only after this point the wettability alteration takes effect, starting near the inlet, resulting in subsequent spontaneous oil invasions. We refer to this limiting case as Slow Wetting Boundary (SWB).

3.1. Berea Sandstone Network

We simulate the above PD/WE model on the homogeneous Berea network. The base-case parameters of the simulations are: P_c^{max}=6600 kPa; Q=5e−13 m^3/s; C_0=500 $^{mg}/_{L}$; Δ_t^{TR}=0.007 s; P=0.01; D=1e−5 cm^2/s; K=1 L/mg; Γ_{max}=0.3 mg/m^2; β=0.0083. Note that the chosen β, K, P, and C_0 parameters correspond to θ_{max}=80° (equation (16)). Although our base-case parameters have not been derived from a particular experiment, they are physically realistic, chosen in order to scan all the possible outcomes of our model during the sensitivity analysis that will follow.

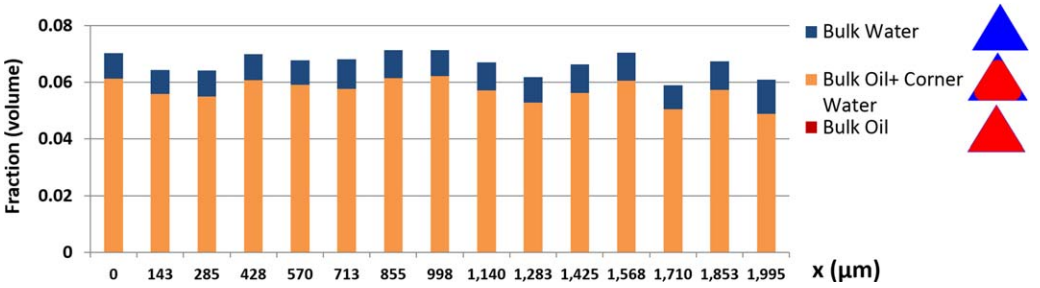

Figure 1. Pore occupancies for the Berea network shown on the *x* axis (parallel to flow, from (left) inlet to (right) outlet) following PD (i.e., PD/WE at $\theta_{max}=0^\circ$). The simulation reached $S_{wi}=0.2$ at P_c^{max} after time $t_f=53$ min.

We first start with the case where polar compounds remain in the oil phase (no partitioning, $P=0$), hence they do not react with the surface, i.e., $\theta_{max}=0$ (equation (16)). This corresponds to a conventional PD simulation at a predefined P_c^{max}. The pore occupancies are shown in Figure 1. Note that in the absence of wetting changes, the water saturation reaches $S_{wi}=0.2$, after which no more invasions are possible at fixed P_c^{max}.

We now run the PD/WE model for the base-case parameters. Two effects are opposing each other in terms of changing S_{wi} following the PD/WE model. On the one hand, the corner water collapse in oil-filled pores due to the contact angle change, as described in section 2.3.5.1, results in a loss in water phase connectivity. This effect, that we call "trapping," tends to increase S_{wi}. On the other hand, the decrease of entry pressures, P_E, due to the contact angle change as described in section 2.3.5.2, results in a gain in entry pressure accessibility. This effect, that we call "enterability," tends to counterbalance the "trapping" effect by decreasing S_{wi}. It follows from the definitions that both the "enterability" and "trapping" effects increase with θ_{max}.

The pore occupancies and wettability change following PD/WE at intermediate-wet conditions ($\theta_{max}=80^\circ$) are shown in Figure 2. The PD/WE at $\theta_{max}=80^\circ$ results in a slightly higher $S_{wi}=0.22$ compared to the PD $S_{wi}=0.2$, meaning that the "trapping" effect is slightly dominating in this case. Note that for $\theta_{max}=80^\circ$, the majority of the remaining corner water at t_f (shown in Figure 2b, top) must be trapped. Indeed, most of the corner half-angles γ are larger than 10°, thus according to equation (17), the corner films should have been expelled if there was any outlet connection. It is clear from the transition Figure 2a (bottom) to Figure 2b (top) that the wettability change occurs preferentially near the inlet at the beginning of the simulation, with the contact angle values, θ, ranging from 0 to θ_{max}. This qualitatively reproduces the early wetting alteration observed by *Bennett et al.* [2004] using FESEM imaging on surfaces near the inlet. Eventually, the adsorption steady state is reached at t_f where a single contact angle θ_{max} governs the pore space.

3.1.1. Effect of θ_{max} on S_{wi}

The pore occupancies and wettability change following PD/WE at water-wet conditions ($\theta_{max}=30^\circ$) are shown in Figure 3. Note that at this relatively low θ_{max}, corner water mostly persists and is not trapped. This is shown in the pore occupancies (Figure 3, top). Consequently, the "trapping" effect is inhibited in this case, which leaves the "enterability" effect. Thus, quite a modest change in wetting in the PD/WE model in this case has led to the value of $S_{wi}=0.14$, i.e., the invasion of an additional $\Delta S_o=0.06$ above the PD oil saturation. Note that the pore occupancies at $t_f=280$ min ($S_{wi}=0.14$ at P_c^{max}) are similar to the $\theta_{max}=0^\circ$ case shown in Figure 1, and the wetting change is analogous to that showed in Figure 2b (bottom).

The pore occupancies shown on the pore-size distribution (PSD) in Figure 4 demonstrate quite clearly that the PD/WE model enables the oil to reach the smallest pores that would not have been accessible following the conventional PD ($\theta_{max}=0^\circ$) at the same fixed P_c^{max}.

3.1.2. Effect of Γ_{max} on S_{wi}

We now keep θ_{max} as the base-case value (80°) and increase Γ_{max} from 0.3 to 1.5 $\frac{mg}{m^2}$, i.e., induce a slower wetting change relative to oil invasion by requiring a higher polar component adsorption level to alter the contact angle. It is clear from the pore occupancy and wettability change in Figure 5a that, during the PD/WE process, the oil front is well ahead of the wettability alteration front in the direction of flow. This behavior is different from that shown for the base case in Figure 2a where the two processes are clearly more synchronized. This higher Γ_{max} results in the "trapping" effect being delayed and its effect being weaker. Since the "enterability" effect is insensitive to Γ_{max}, only depending on θ_{max}, this results in $S_{wi}=0.09$ being

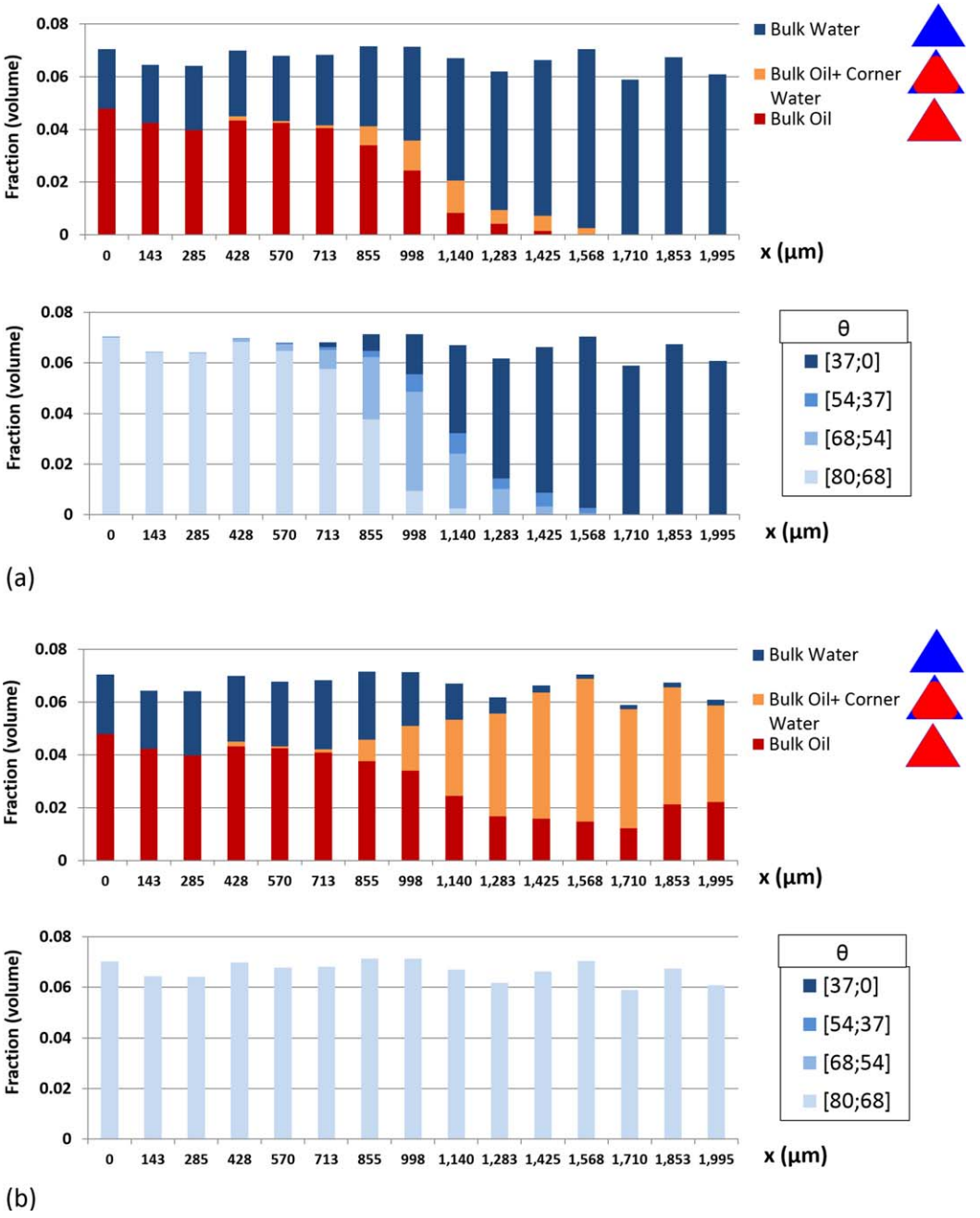

Figure 2. (top) Pore occupancies and (bottom) wetting change for the Berea network shown on the *x* axis (parallel to flow, from (left) inlet to (right) outlet) following PD/WE for the base-case parameters after (a) $t_{1/2}=31$ min (at which $S_w \approx \frac{S_{wi}+1}{2}$) and (b) $t_f=315$ min ($S_{wi}=0.22$ at P_c^{max}).

significantly lower than the base-case value (0.22). Note that the final wettability distribution at t_f is similar to that shown in Figure 2b, bottom.

We now aim to link the simulations to the behavior observed by *Bennett et al.* [2004] in their core-flood experiment. To do so, we focus on the evolution of the average mobile concentration of polar compounds in the oil phase at the outlet bonds, depending on the system's adsorptive capacity, as described by Figure 6a. For the "No partitioning" case, describing a conventional PD process where polar compounds do not partition from the oil into the water phase, these polar species naturally emerge at the outlet at their maximum concentration and exactly when oil breaks through ($t=707$ s). Besides, when the adsorptive capacity,

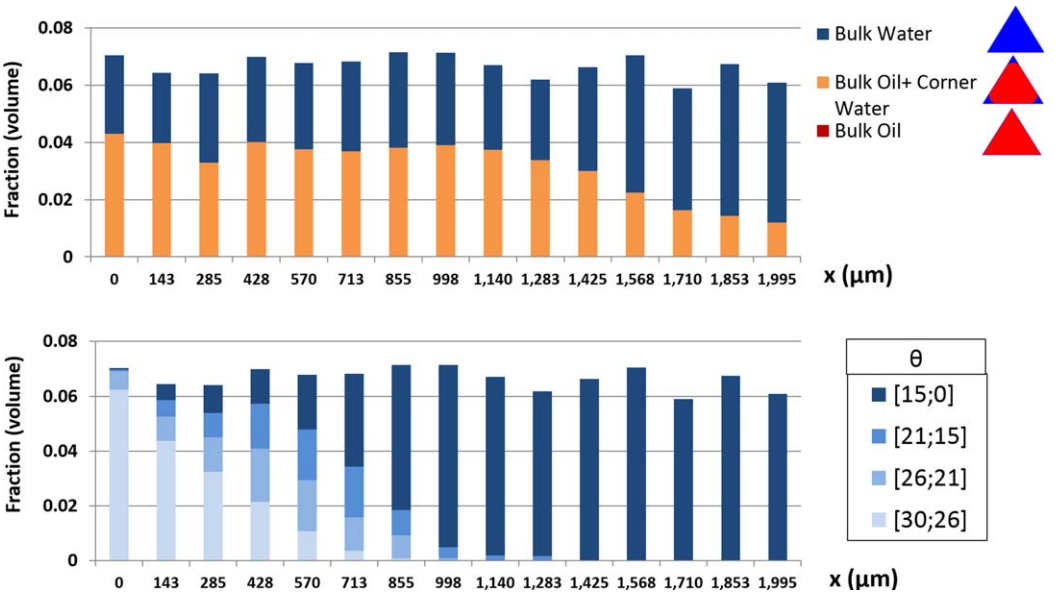

Figure 3. (top) Pore occupancies and (bottom) wetting change for the Berea network shown on the *x* axis (parallel to flow, from (left) inlet to (right) outlet) following PD/WE at $\theta_{max}=30^{\circ}$ and $\Gamma_{max}=0.3\ \frac{mg}{m^2}$ after $t_{1/2}=29$ min (at which $S_w \approx \frac{S_{wi}+1}{2}$).

Γ_{max}, increases, we observe a clear delay in the appearance of polar compounds at the outlet due to a higher surface activity. Note that the high concentration at which they appear for the $\Gamma_{max}=0.03\ \frac{mg}{m^2}$ case is mainly a contribution of the oil invasion process which carries polar compounds all through the network in the absence of any substantial surface activity, as described in section 2.1. For higher Γ_{max}, when the adsorptive capacity of the system is significant, the oil phase appears at the outlet depleted of polar species, which are then resupplied from the inlet through a diffusion process, as described in section 2.2. The simulations qualitatively reproduce the experimental trends provided in Figure 6b, with the polar species "fluoren-9-one," "carbazole," "benzocarbazole," and "p-cresol" corresponding to an increasing surface activity (i.e., higher Γ_{max}), in order. Note that each curve's endpoint in Figure 6a corresponds to the adsorption steady state being reached. At the latter, all the pores in the network have reached maximum adsorption levels, hence maximum wetting change, regardless of the final mobile concentrations. Ultimately, the

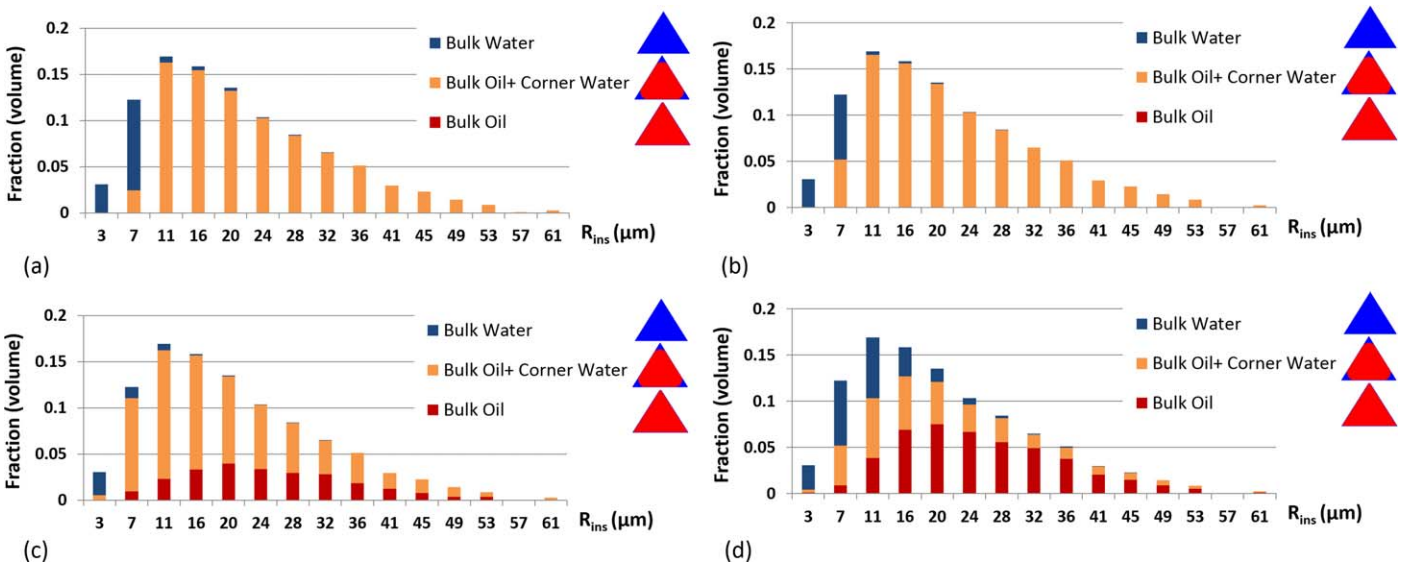

Figure 4. Pore occupancies for the Berea network shown on the pore-size distribution following PD/WE at $\Gamma_{max}=0.3\ \frac{mg}{m^2}$ for (a) $\theta_{max}=0^{\circ}$ ($S_{wi}=0.2$); (b) $\theta_{max}=30^{\circ}$ ($S_{wi}=0.14$); (c) $\theta_{max}=60^{\circ}$ ($S_{wi}=0.05$); and (d) $\theta_{max}=80^{\circ}$ ($S_{wi}=0.22$).

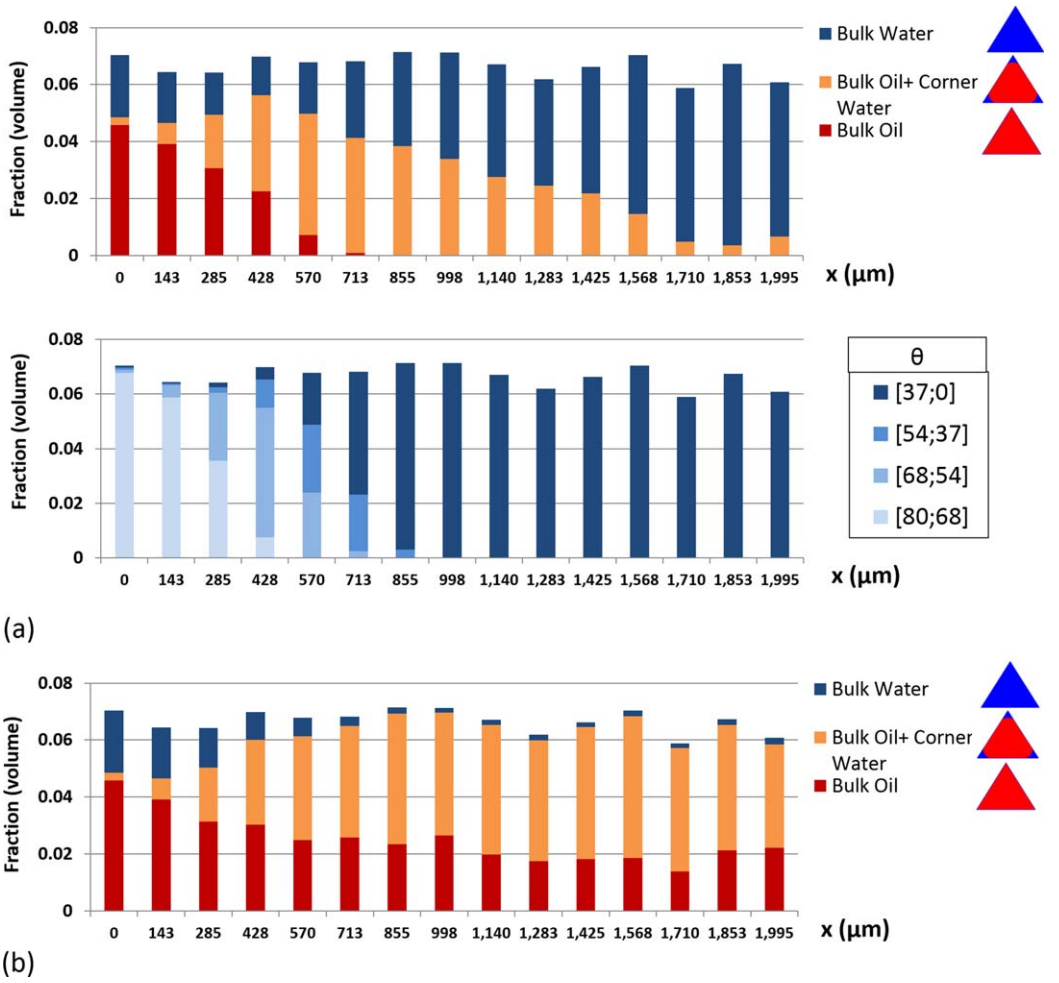

Figure 5. (a) Pore occupancies and (bottom) wetting change for the Berea network shown on the *x* axis (parallel to flow, from (left) inlet to (right) outlet) following PD/WE at $\theta_{max}=80^\circ$ and $\Gamma_{max}=1.5\ \frac{mg}{m^2}$ after $t_{1/2}=32$ min (at which $S_w \approx \frac{S_{wi}+1}{2}$) and (b) pore occupancies (only) at $t_f=433$ min ($S_{wi}=0.09$ at P_c^{max}).

average mobile concentration of polar compounds in the oil phase at the outlet bonds (normalized by C_0), $\widehat{C_{outlet}}$, will reach its maximum value, equal to 1, but this will not affect the final contact angles and initial water saturation attained.

The pore occupancies shown on the pore-size distribution in Figure 7, combined with Figure 4d (for $\Gamma_{max}=0.3\frac{mg}{m^2}$), reveal that a slower wetting change relative to oil invasion, i.e., higher Γ_{max} at intermediate-wet conditions leads to a larger volume of small pores being invaded following PD/WE as the invasion process is driven further due to a weaker "trapping" effect.

3.1.3. Combined Effect of θ_{max} and Γ_{max} on S_{wi}

The combined effects of θ_{max} and Γ_{max} on S_{wi} at fixed P_c^{max} are summarized in Figure 8. Note that the case $\theta_{max}=0^\circ$, corresponding to the conventional PD, is shown for comparison purposes, as the notion of Γ_{max} is not applicable in the absence of adsorption. The results are clearly nonmonotonic with regard to θ_{max}, which can be interpreted by the competition between the two opposing effects: "enterability" and "trapping," as follows:

1. For intermediate-wet conditions ($\theta_{max}=80^\circ$), where both the "trapping" and "enterability" effects are significant, S_{wi} monotonically decreases with faster oil invasion relative to wetting change, i.e., higher Γ_{max}. Indeed, S_{wi} decreases from a value of 0.41, significantly higher than the $\theta_{max}=0^\circ$ case (0.2), to a value as low as 0.09. This, as explained above, is due to the "trapping" effect getting delayed at higher Γ_{max}.
2. Switching to weakly water-wet conditions ($\theta_{max}=60^\circ$), leads to much lower S_{wi}, with the gap narrowing at high Γ_{max}. In fact, while both the "enterability" and "trapping" effects get weaker, the loss in "enterability" is lower than the decrease in "trapping," meaning that the former dominates.

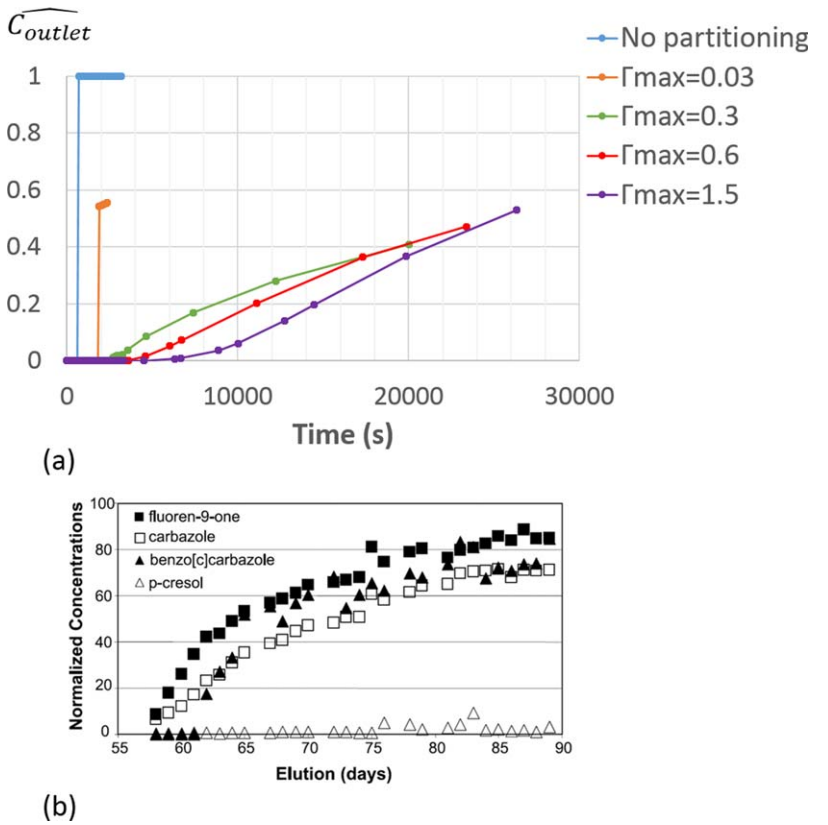

Figure 6. (a) Simulated evolution in time of the average mobile concentration of polar compounds in the oil phase at the outlet bonds (normalized by C_0), $\widehat{C_{outlet}}$, for the different $\Gamma_{max}\left[\frac{mg}{m^2}\right]$ imposed, compared to the "No partitioning" case, for the Berea network; (b) experimental plot of the normalized concentrations of polar compounds in the produced oil (mobile) function of the elution time [*Bennett et al.*, 2004].

3. For water-wet conditions ($\theta_{max}=30°$) where "trapping" is inhibited, S_{wi} is not sensitive to Γ_{max}. This is reasonable since by slowing down the wettability alteration compared to the oil invasion, only the pore-filling sequence is likely to change due to the wettability alteration. And in the absence of any generated trapping, this does not affect the final S_{wi}.
4. Finally, by uniformly distributing $\theta_{max} \in [0, 80°]$, the resulting "$S_{wi}$ versus Γ_{max}" curve lies between the $\theta_{max}=60$ and 80° cases.

Note that S_{wi} for both $\theta_{max}=60$ and 80° reside between their respective slow and fast wetting boundaries (SWB and FWB, respectively), as expected. Moreover, while the FWB increases with higher θ_{max} due to a more important "trapping" effect, the SWB coincides for the two contact angles considered.

The predicted effects of the PD/WE model on conventional calculations of the oil column saturations are now described. The S_w versus height, h, above the oil water contact (OWC) is traditionally calculated using

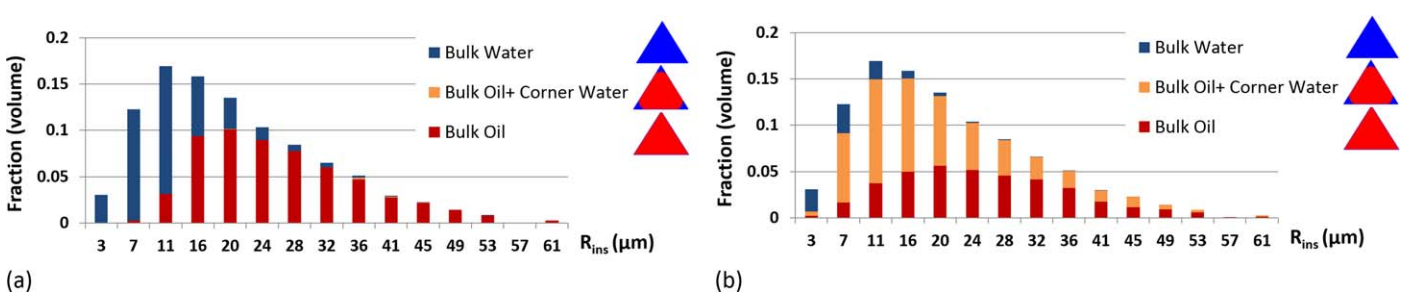

Figure 7. Pore occupancies for the Berea network shown on the pore-size distribution following PD/WE at $\theta_{max}=80°$ for (a) $\Gamma_{max}=0.03$ ($S_{wi}=0.42$) and (b) $\Gamma_{max}=1.5$ $\frac{mg}{m^2}$ ($S_{wi}=0.09$).

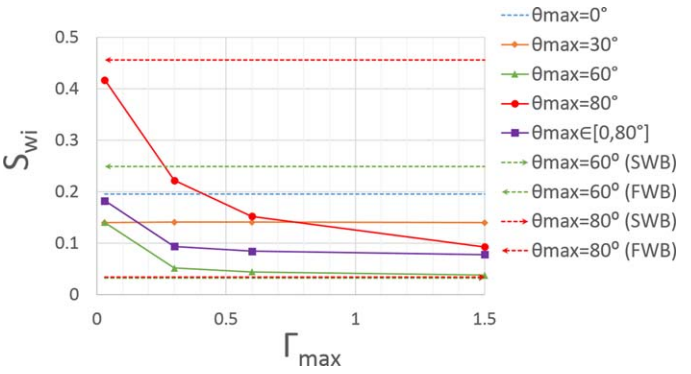

Figure 8. The effect of Γ_{max} on S_{wi} for different θ_{max} values for the Berea network. FWB and SWB are the limiting fast wetting and slow wetting boundaries, respectively.

the PD curve, and this is shown in Figure 9 (denoted $\theta_{max}=0°$). A series of simulations of the PD/WE model were carried out by varying the main pair of parameters $(\theta_{max}, \Gamma_{max})$ at different P_c^{max} values, each corresponding to a different height,h, in the oil column (Figure 9). Note that $h=3.3$ m corresponds to the base-case P_c^{max} (6600 Pa) used for previous simulations. By applying the PD/WE model $(\theta_{max} > 0°)$, significant changes in phase saturations occur within the oil column, depending on θ_{max} and Γ_{max}. This is a generalization of the discussion related to Figure 8 in essence, where it would apply in the oil column as the oil charges the reservoir and the process of wettability evolution occurs.

1. For $\theta_{max}=80°$, the curves for the different chosen Γ_{max} lie between the boundaries FWB and SWB, with higher Γ_{max} leading to monotonically lower S_{wi}. Additionally, the model may result in significant nonzero water saturations, even high in the oil column. In fact, for a relatively fast wetting change $(\Gamma_{max}=0.03)$, we observe a vertical curve. This is due to the significant amount of water trapping being created at a relatively early stage that inhibits any further displacement, independent of how high the attained P_c^{max} (or h) becomes.
2. The $\theta_{max}=60°$ curves follow the same behavior as the $\theta_{max}=80°$ case, but with a narrower gap between these curves as FWB is shifted to the left. Indeed, a less important "trapping" effect compared to the previous case leads to S_{wi} being lower all along the oil column. Note that the two slow wetting boundaries (SWB) for $\theta_{max}=60$ and $80°$ coincide.
3. The $\theta_{max}=30°$ curve, which is insensitive to Γ_{max}, is shifted to the left as compared to the conventional PD curve. In other words, PD/WE at water-wet conditions leads to lower water saturations all along the oil column. In fact, even at the highest point of the curve where all the pores are prone to invasion at $\theta_{max}=0°$, S_{wi} is slightly lower due to the shrinking of water in the corners.

3.2. Carbonate Network

In this section, we consider calculations of the type presented above, but now for the more complex multiscale carbonate. The base-case parameters of the simulations are: $P_c^{max}=11713$ kPa; $Q=5e-13$ m^3/s; $C_0=500$ mg/L; $\Delta_t^{TR}=0.007$ s; $P=0.01$; $D=1e-5$ cm^2/s; $K=1$ L/mg; $\Gamma_{max}=0.47$ mg/m^2; $\beta=0.0083$. Again, the chosen β, K, P, and C_0 correspond to $\theta_{max}=80°$ (equation (16)). Note that we chose the P_c^{max} base-case value for the carbonate network to be significantly higher than that for the Berea network. Indeed, the carbonate network has far smaller pores, thus requires higher capillary pressures to achieve water saturations comparable to those presented for the Berea network. The Γ_{max} base-case value was slightly adjusted accordingly.

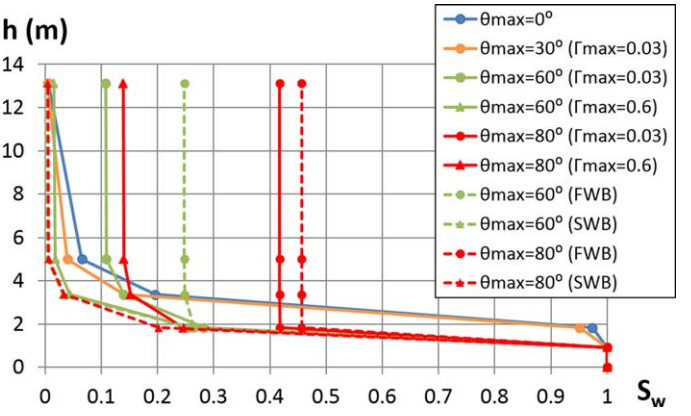

Figure 9. Distribution in the oil column following the application of the PD/WE model for different combinations of θ_{max} and Γ_{max} $\left[\frac{mg}{m^2}\right]$ values in the Berea network. FWB and SWB are the limiting fast wetting and slow wetting boundaries, respectively.

3.2.1. Effect of θ_{max} on S_{wi}

The pore occupancies shown on the pore-size distribution after the application of PD/WE at different θ_{max} are shown in Figure 10. The PD/WE model at higher θ_{max} enables the oil to reach higher oil saturations and to invade smaller pores.

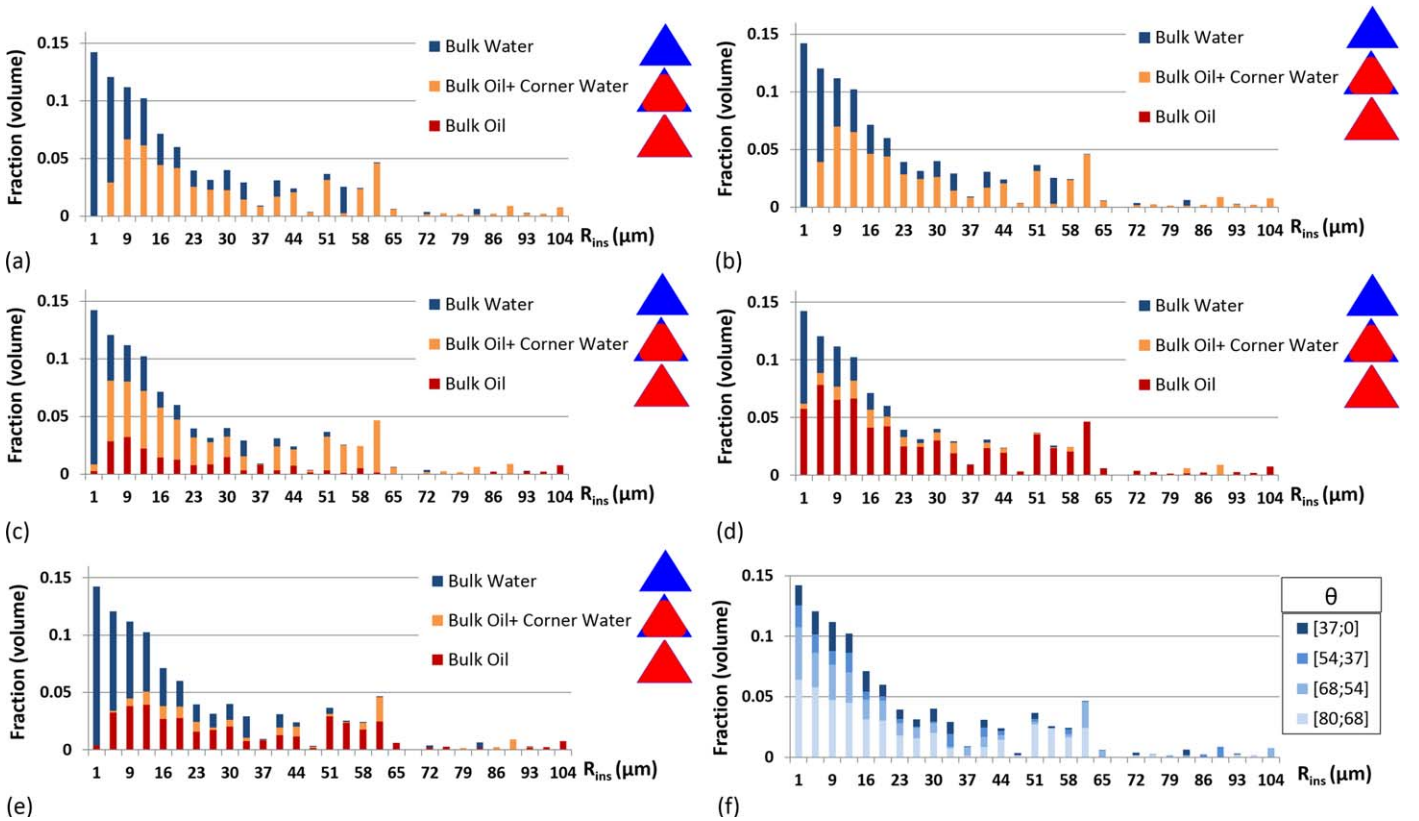

Figure 10. Pore occupancies for the carbonate network shown on the pore-size distribution following PD/WE at $\Gamma_{max}=0.47\frac{mg}{m^2}$ for (a) $\theta_{max}=0^\circ$ ($S_{wi}=0.5$); (b) $\theta_{max}=30^\circ$ ($S_{wi}=0.46$); (c) $\theta_{max}=60^\circ$ ($S_{wi}=0.32$); (d) $\theta_{max}=80^\circ$ ($S_{wi}=0.22$); and (e) $\theta_{max}=80^\circ$ stopped at a predefined $S_w=0.5$. (f) The wettability alteration shown on the pore-size distribution corresponding to Figure 10e.

In particular, it allows oil migration into micropores (first bin of the PSD) for high enough θ_{max} (60 and 80°). Indeed, these micropores were not accessible otherwise ($\theta_{max} < 60^\circ$) at the same fixed P_c^{max}. As shown in Figure 10e, the filling of micropores at $\theta_{max}=80^\circ$ occurred early in the process at S_w lower than 0.5, which coincides with S_{wi} for the conventional PD (Figure 10a). Indeed, at the same water saturation, the filling

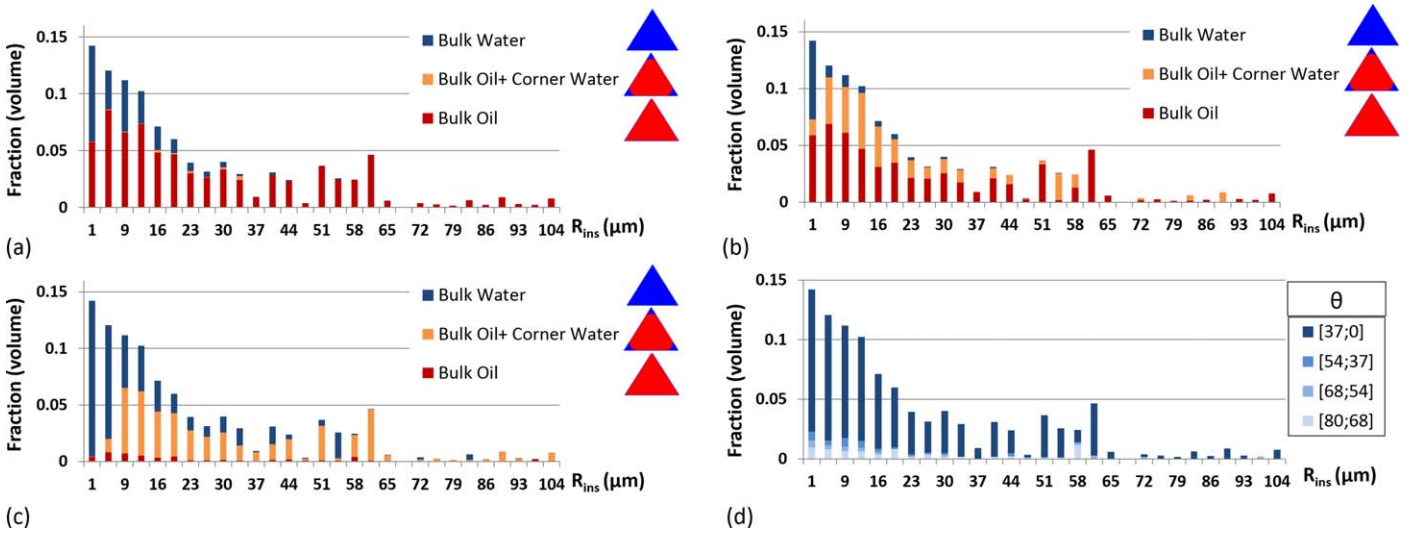

Figure 11. Pore occupancies for the carbonate network shown on the pore-size distribution following PD/WE at $\theta_{max}=80^\circ$ for (a) $\Gamma_{max}=0.1$ ($S_{wi}=0.26$); (b) $\Gamma_{max}=1.4$ ($S_{wi}=0.13$); and (c)$\Gamma_{max}=1.4\ \frac{mg}{m^2}$ stopped at a predefined $S_w=0.5$. (d) The wettability alteration shown on the pore-size distribution corresponding to Figure 11c.

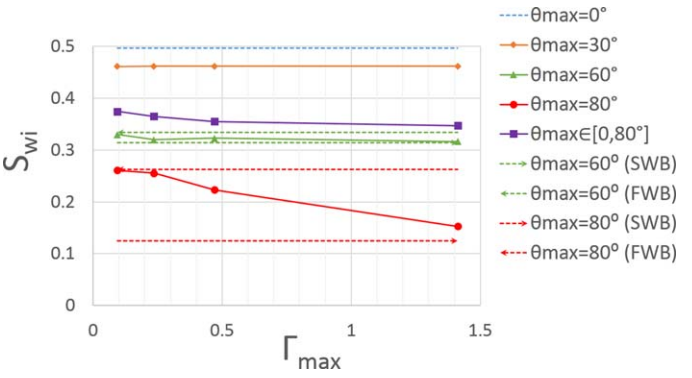

Figure 12. The effect of Γ_{max} $\left[\frac{mg}{m^2}\right]$ on S_{wi} for different θ_{max} values for the carbonate network. FWB and SWB are the limiting fast wetting and slow wetting boundaries, respectively.

pattern when applying PD/WE at intermediate-wet conditions compared to the conventional PD is different as the oil invasion is more spread over the PSD. This is due to the dramatic decrease in entry pressures following the increase in contact angles from 0° to θ_{max}=80° (Figure 10f), which changes the filling sequence to become less dependent on pore size and more linked to the adsorption level of polar compounds and the resulting wettability alteration.

3.2.2. Effect of Γ_{max} on S_{wi}

In this section, we keep θ_{max} as the base-case value (80°) and induce a slower wetting change relative to oil invasion by increasing Γ_{max} from 0.1 to 1.4 $\frac{mg}{m^2}$. The pore occupancies shown on the pore-size distribution in Figure 11, added to the information from Figure 10d, confirm the earlier findings that a slower wetting change relative to oil invasion at intermediate-wet conditions results in monotonically decreasing S_{wi} at the same predefined P_c^{max}. Besides, according to Figure 11d, although the wettability alteration was delayed for a higher Γ_{max} (compared to Figure 10f), the invasion of micropores still occurred at $S_w < 0.5$ (Figure 11d). Indeed, those invaded micropores experienced enough wettability alteration for their P_E to sufficiently decrease at a relatively early stage. Eventually, oil migrates further into micropores for higher Γ_{max}.

3.2.3. Combined Effect of θ_{max} and Γ_{max} on S_{wi}

We summarize the combined effects of θ_{max} and Γ_{max} on S_{wi} at fixed P_c^{max} in Figure 12. The results are qualitatively similar to those for the Berea network (Figure 8). However, the dependency of S_{wi} on the balance between the oil invasion and wettability alteration processes at fixed θ_{max} is weaker for the carbonate network because the "trapping" effect is less significant. This pattern is attributed to the particular topology of the multiscale carbonate network where the microporosity joins up the otherwise disconnected larger pores. Indeed, the largest pores are naturally invaded first during PD, and many lose their corner water generating a loss in the water phase connectivity. However, because their contribution to the overall network connectivity is low, water remains largely connected early on, leading eventually to lower S_{wi}.

More generally, by varying P_c^{max}, we obtain the oil column distributions for the different pairs of parameters $(\theta_{max}, \Gamma_{max})$ shown in Figure 13. Note that h=6 m corresponds to the base-case P_c^{max} (11712 Pa) utilized for all previous simulations. Again, the results of the PD/WE model follow the same qualitative trends exhibited by the Berea network in Figure 9, but the gap between the curves at fixed θ_{max} (60 or 80°) is narrower since the fast wetting boundary, FWB, is shifted to the left. This is again due to the weaker "trapping" effect.

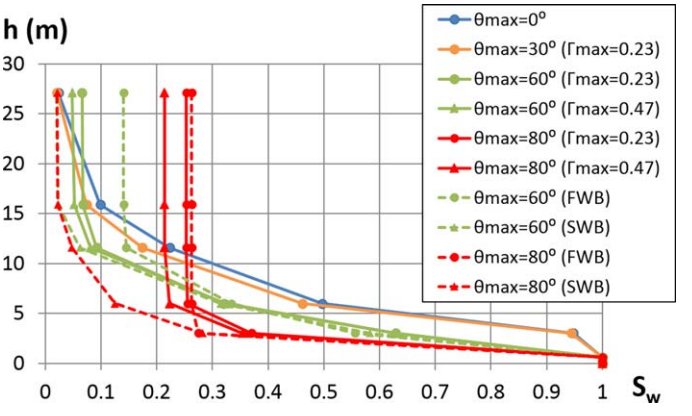

Figure 13. Distribution in the oil column following the application of the PD/WE model for different combinations of θ_{max} and Γ_{max} $\left[\frac{mg}{m^2}\right]$ values in the carbonate network. FWB and SWB are the limiting fast wetting and slow wetting boundaries, respectively.

4. Conclusions

In this paper, we have developed a novel pore-scale model where the wetting state evolves during primary drainage, referred to as the Primary Drainage/Wettability Evolution (PD/WE) model. The model involves small polar species from the oleic phase with high solubility in water and important surface activity (e.g., alkylphenols and

carbazoles). The PD/WE model qualitatively reproduced experimental observations reported by *Bennett et al*. [2004] where an early rapid wettability alteration occurred during primary drainage, preferentially near the inlet, due to the adsorption of these polar species.

The PD/WE model is proposed as a physically well-founded *plausible* model using all the pore-scale physics of fluid displacements and wetting alteration that we currently understand. We are applying this to generate understanding and explanations of how the complex range of parameters interact in the primary drainage and wetting change process that occur when crude oil invades a porous rock. The possible fluid configurations and wetting states that can occur and how these give rise to the postdrainage oil column are considered and explained. Furthermore, we also intended to show that it is straightforward for oil to invade very small water-filled, initially water-wet pores with both reasonable and minimal physics-based assumptions.

Upon the application of the wettability alteration model, we highlighted that two effects were competing to determine the water saturation following primary drainage, S_{wi}, at fixed maximum capillary pressure,$P_c^{\max}$:

1. "Trapping": loss in water phase connectivity due to corner water removal following the wettability alteration in oil-filled pores, which tends to increase S_{wi}. Compared to the Berea network, this effect was generally weaker in the carbonate network due to its particular connectivity dominated by its microporosity.
2. "Enterability": decrease in pore entry pressure P_E following the wetting change of water-filled pores, which tends to decrease S_{wi}.

We invoked clear differences in the PD behavior by varying both the level of wettability alteration (through the imposed maximum contact angle reached, $\theta_{\max}$) and the balance between the oil invasion and wetting change processes (through the system's adsorptive capacity, $\Gamma_{\max}$). These two parameters proved to dictate S_{wi} following PD/WE as they vary the competition between "trapping" and "enterability" as follows:

1. For intermediate-wet conditions ($\theta_{\max}=80^\circ$), where both the "trapping" and "enterability" effects are significantly strong, S_{wi} monotonically decreased with faster oil invasion relative to wetting change (higher $\Gamma_{\max}$) due to the resulting delay in "trapping." In fact, depending on $\Gamma_{\max}$, the model may end up with either lower or significantly higher S_{wi} throughout the oil column compared to the traditional PD simulation. This change in S_{wi} was less dramatic for the carbonate network than for the Berea network because of the "trapping" being weaker in the former.
2. For weakly water-wet conditions ($\theta_{\max}=60^\circ$), although the behavior was similar to the 80° case, S_{wi} was generally lower. In fact, while both the "enterability" and "trapping" effects get weaker with lower contact angle, the loss in "enterability" is compensated by a stronger decrease in "trapping," meaning that the former generally dominates.
3. For water-wet conditions $(\theta_{\max}=30^\circ)$ where "enterability" dominates in the absence of "trapping," S_{wi} was independent of $\Gamma_{\max}$ and was lower all along the oil column compared to the traditional PD.

The PD/WE model provides a physically plausible scenario to explain the phenomenon of oil invasion into micropores. Indeed, we demonstrated that in the cases of relatively fast oil invasion or small wetting changes, the oil was able to reach significantly higher saturations at fixed $P_c^{\max}$. Particularly in the carbonate network, oil did invade the micropores at moderate capillary pressure values following their wetting alteration. In fact, these micropores were not accessible otherwise following the conventional PD at the same fixed $P_c^{\max}$. The model may also be used to describe carbon-dioxide storage and NAPL contamination in aquifers. In the latter application wetting changes are expected to play an important role due to adsorption of various compounds.

Acknowledgments
The authors are grateful to the members of the ITF consortium, DONG energy, Wintershall, BG Group, and Chevron, for funding part of this work. We would also like to thank Zeyun Jiang for providing the networks data set. The data presented in this paper are available upon request via R.van_Dijke@hw.ac.uk.

References

Al-Yousef, H. Y., P. M. Lichaa, A. U. Al-Kaabi, and H. Alpustun (1995), Wettability evaluation of a carbonate reservoir rock from core to pore level, paper 29885 presented at Middle East Oil Show, Soc. of Pet. Eng., Manama.

Bennett, B., J. O. Buckman, B. F. J. Bowler, and S. R. Larter (2004), Wettability alteration in petroleum systems: The role of polar non-hydrocarbons, *Pet. Geosci.*, *10*(3), 271–277, doi:10.1144/1354-079303-606.

Blunt, M. J., and H. Scher (1995), Pore-level modeling of wetting, *Phys. Rev. E*, *52*(6), 6387.

Buckley, J. S., and Y. Liu (1998), Some mechanisms of crude oil/brine/solid interactions, *J. Pet. Sci. Eng.*, *20*(3–4), 155–160, doi:10.1016/S0920-4105(98)00015-1.

Cantrell, D. L., and R. M. Hagerty (1999), Microporosity in Arab formation carbonates, Saudi Arabia, GeoArabia, *4*, 129–154.

Clerke, E. A. (2009), Permeability, relative permeability, microscopic displacement efficiency and pore geometry of M_1 bimodal pore systems in Arab-D limestone, *SPE J.*, *14*(3), 524–531, doi:10.2118/105259-PA.
Clerke, E. A., et al. (2014), Wireline spectral porosity analysis of the Arab limestone—From Rosetta Stone to Cipher, paper presented at SPWLA 55th Annual Logging Symposium, Soc. of Petrophys. and Well-Log Anal., Abu Dhabi.
Dodd, N., et al. (2014), Pore-scale imaging of oil and wettability in native-state, mixed-wet reservoir carbonates, paper presented at International Petroleum Technology Conference, Int. Pet. Technol., Doha.
Fassi-Fihri, O., M. Robin, and E. Rosenberg (1995), Wettability studies at the pore level: a new approach by the use of cryo-scanning electron microscopy, *SPE Form. Eval.*, *10*(1), 11–19, doi:10.2118/22596-PA.
Fung, L. S. K., U. Middya, and A. H. Dogru (2011), Numerical simulation of fractured carbonate reservoirs with the M_1 bimodal pore system, paper presented at SPE Reservoir Simulation Symposium, Soc. of Pet. Eng., The Woodlands, Tex.
Harland, S. R., R. A. Wood, A. Curtis, M. I. J. van Dijke, K. Stratford, Z. Jiang, W. Kallel, and K. Sorbie (2015), Quantifying flow in variably wet microporous carbonates using object-based geological modelling and both lattice-Boltzmann and pore network fluid flow simulations, AAPG Bull., *99*(10), pp. 1827–1860, doi:10.1306/04231514122.
Huang, Y., P. S. Ringrose, K. S. Sorbie, and S. R. Larter (1996), The effects of heterogeneity and wettability on oil recovery from laminated sedimentary structures, *SPE J.*, *1*(04), 451–462, doi:10.2118/30781-PA.
Jiang, Z., K. Wu, G. Couples, M. I. J. van Dijke, K. S. Sorbie, and J. Ma (2007), Efficient extraction of networks from three-dimensional porous media, *Water Resour. Res.*, *43*, W12S03, doi:10.1029/2006WR005780.
Jiang, Z., M. I. J. van Dijke, K. S. Sorbie, and G. D. Couples (2013), Representation of multiscale heterogeneity via multiscale pore networks, *Water Resour. Res.*, *49*, 5437–5449, doi:10.1002/wrcr.20304.
Kallel, W., M. I. J. van Dijke, K. S. Sorbie, R. Wood, Z. Jiang, and S. Harland (2015), Modelling the effect of wettability distributions on oil recovery from microporous carbonate reservoirs, *Adv. Water Resour.*, *95*, 317–328, doi:10.1016/j.advwatres.2015.05.025.
Knackstedt, M. A., W. V. Pinczewski, A. Fogden, and T. Senden (2011), Improved characterization of EOR processes in 3D. Characterizing mineralogy, wettability and residual fluid phases at the pore scale, paper presented at SPE Enhanced Oil Recovery Conference, Soc. of Pet. Eng., Kuala Lumpur.
Kovscek, A. R., H. Wong, and C. J. Radke (1993), A pore-level scenario for the development of mixed wettability in oil reservoirs, *AIChE J.*, *39*(6), 1072–1085, doi:10.1002/aic.690390616.
Lucach, S. O., B. F. J. Bowler, N. Frewin, and S. R. Larter (2002), Variation in alkylphenol distributions in a homogenous oil suite from the Dhahaban petroleum system of Oman, *Org. Geochem.*, *33*(5), 581–594, doi:10.1016/S0146-6380(02)00014-1.
Marathe, R., M. L. Turner, and A. Fogden (2012), Pore-scale distribution of crude oil wettability in carbonate rocks, *Energy Fuels*, *26*(10), 6268–6281, doi:10.1021/ef301088j.
Ryazanov, A. V., K. S. Sorbie, and M. I. J. van Dijke (2014), Structure of residual oil as a function of wettability using pore-network modelling, *Adv. Water Resour.*, *63*, 11–21, doi:10.1016/j.advwatres.2013.09.012.
Taylor, P., S. Larter, M. Jones, J. Dale, and I. Horstad (1997), The effect of oil-water-rock partitioning on the occurrence of alkylphenols in petroleum systems, *Geochim. Cosmochim. Acta*, *61*(9), 1899–1910, doi:10.1016/S0016-7037(97)00034-3.
van Duin, A. C. T., and S. R. Larter (2001), A computational chemical study of penetration and displacement of water films near mineral surfaces, *Geochem. Trans.*, *2*(6), 35–44, doi:10.1039/b105078h.